Journal of Magnetic Resonance **156,** 10–18 (2002)
doi:10.1006/jmre.2002.2539

Correlation of Backbone Amide and Side-Chain ^{13}C Resonances in Perdeuterated Proteins

Frank Löhr[1] and Heinz Rüterjans

Institut für Biophysikalische Chemie, Johann Wolfgang Goethe-Universität Frankfurt, Biozentrum N230, Marie Curie-Strasse 9, 60439 Frankfurt am Main, Germany

Received August 13, 2001; revised March 20, 2002; published online May 31, 2002

Side-chain carbon resonance assignments are difficult to obtain for larger proteins. While standard methods require protons for excitation and detection of magnetization, their presence is often unacceptable and often leads to unacceptable relaxation losses at the directly bound carbon sites. In this paper, pulse sequences are presented which provide connectivities between aliphatic side-chain ^{13}C and amide ^{1}H and ^{15}N chemical shifts in fully deuterated, $^{13}C/^{15}N$-enriched proteins. Magnetization either starts off from carbons or from both nitrogens and protons and is passed along the side-chain via ^{13}C–^{13}C isotropic mixing. Direct rather than ^{13}CO-relayed $^{15}N \rightarrow {}^{13}C^{\alpha}$ or $^{13}C^{\alpha} \rightarrow {}^{15}N$ transfer steps allow the detection of intraresidual as well as sequential correlations. To avoid ambiguities between these two types in the three-dimensional version of the experiments, a fourth dimension can be introduced to achieve their separation along a $^{13}C^{\alpha}$ frequency axis. The novel methods are demonstrated with the uniformly $^{2}H/^{13}C/^{15}N$ labeled 35-kDa protein diisopropylfluorophosphatase from *Loligo vulgaris*.

Key Words: **CC-TOCSY; DFPase; isotopic labeling; triple resonance NMR; TROSY.**

INTRODUCTION

Deuteration leads to substantial improvements in NMR spectra of larger proteins in terms of both sensitivity and resolution (see Refs. (*1–3*) for recent reviews). In particular, amide-proton detected triple resonance experiments applied to $^{2}H/^{13}C/^{15}N$ labeled proteins benefit from the elimination of the efficient ^{1}H, ^{1}H, and ^{1}H, ^{13}C dipolar (DD) spin relaxation pathways (*4, 5*). Advantages of deuteration are even more pronounced when triple resonance spectroscopy is combined with [^{15}N, ^{1}H]-TROSY (*6*), which relies on the destructive interference of the remaining dominant contributions to relaxation, $^{1}H^{N}$, ^{15}N DD, and $^{1}H^{N}$ or ^{15}N chemical shift anisotropy (CSA). TROSY-based triple resonance methods therefore enabled assignments of proteins with molecular weights of up to 110 kDa to be obtained (*7–12*). Such assignments are almost invariably limited to backbone and $^{13}C^{\beta}$ resonances, although further side-chain resonance assignments would be of interest, too, as they are prerequisites for the evaluation of NOESY spectra, the analysis of side-chain dynamics from ^{13}C and ^{2}H relaxation, or simply allow an identification of amino acid types.

For obvious reasons standard HCC(CO)NH-TOCSY pulse sequences (*13–16*) are inappropriate to achieve side-chain resonance assignments of perdeuterated proteins, while they have been successfully applied to 50% (*17*) and 65% (*18*) random fractionally deuterated proteins. However, very high molecular weight proteins will require higher levels of deuteration. It should be mentioned that methyl resonances can be assigned very efficiently (*19, 20*) using $^{2}H/^{13}C/^{15}N$ (^{1}H-methyl)-labeled samples (*21–23*). In a more general approach, suitable for fully deuterated proteins, the (H)CC(CO)NH-TOCSY sequence has been adapted by allowing the magnetization to originate from aliphatic carbons (*24*). Despite the absence of any polarization transferred from protons the sensitivity was sufficient to obtain almost complete aliphatic side-chain ^{13}C assignments for a 96% deuterated 29-kDa protein with an estimated rotational correlation time τ_c of 10.4 ns. With decreasing molecular tumbling rates and increasing magnetic field strengths these carbonyl-relayed backbone-amide–side-chain correlation experiments are expected to suffer from efficient ^{13}CO CSA relaxation during the critical $^{13}C^{\alpha} \rightarrow {}^{13}CO/{}^{13}CO \rightarrow {}^{15}N$ polarization transfer period.

Here we propose alternative methods, not affected by transverse carbonyl relaxation, to link aliphatic side-chain ^{13}C chemical shifts to those of backbone ^{15}N and $^{1}H^{N}$ nuclei in $^{13}C/^{15}N$ enriched, highly deuterated proteins. One obvious way to achieve this goal is to replace the relayed polarization transfer of the CC(CO)NH-TOCSY (*24*) by a direct $^{13}C^{\alpha} \rightarrow {}^{15}N$ transfer step. Of potentially higher utility for larger proteins is an "out-and-back" variant which contains two C–C isotropic mixing periods and exploits amide proton polarization at the outset of the sequence. This strategy lends itself to sensitivity and resolution enhancement via [^{15}N, ^{1}H]-TROSY (*6, 7*), which becomes most efficient at high magnetic fields, where fast ^{13}CO CSA relaxation would deteriorate CC(CO)NH-type experiments.

[1] To whom all correspondence should be addressed. Fax: +49-69-798-29632. E-mail: murph@bpc.uni-frankfurt.de.

1090-7807/02 $35.00

RESULTS AND DISCUSSION

The magnetization transfer pathway of conventional side-chain-to-backbone correlation NMR pulse sequences starts at aliphatic carbon bound protons. At the expense of sensitivity the initial INEPT (*25*) step inevitably has to be omitted for application to perdeuterated proteins, which carry protons only at exchangeable sites. One example is the CC(CA)NH-TOCSY sequence, outlined in Fig. 1, which is derived from HCC(CA)NH-TOCSY type experiments (*14, 18, 26*) and may be viewed as the intraresidual counterpart of the CC(CO)NH-TOCSY (*24*). Briefly, after excitation of aliphatic carbons and chemical shift labeling (t_1) magnetization is passed along the aliphatic carbon skeleton via CC isotropic mixing. In the subsequent $^{13}C \rightarrow {}^{15}N$ polarization transfer, magnetization is relayed to amide nitrogens of the same and the sequentially following residue through $^1J_{NC_\alpha}$ and $^2J_{NC_\alpha}$ couplings, respectively. To avoid a loss of coherence due to passive $^1J_{C_\alpha C_\beta}$ interactions, the duration Δ is tuned to $1/^1J_{C_\alpha C_\beta}$. Nitrogen-15 chemical shifts evolve in time in a semiconstant manner (*14, 36*) as a function of t_2. Finally, magnetization is transferred to amide protons for detection, using a standard sensitivity enhanced reverse INEPT element (*37*) combined with gradient coherence selection (*38*). Optional decoupling of carbon spins during acquisition is recommended as it results in slightly narrower $^1H^N$ lineshapes. Deuterium decoupling must be applied during all periods of transverse ^{13}C magnetization in order to eliminate the effect of the ^2H quadrupolar interaction (*4*), otherwise causing faster relaxation.

Identical correlations can be obtained using the novel (HNCAC)C(C)CANH-TOCSY pulse sequence which is depicted in Fig. 2. The flow of magnetization in the 3D and 4D versions of the experiment can be described as

$$^1H_i^N \rightarrow {}^{15}N_i \rightarrow {}^{13}C_{i,i-1}^{\alpha} \rightarrow {}^{13}C_{i,i-1}^{\alpha\beta\gamma\delta\varepsilon}(t_1) \rightarrow {}^{13}C_{i,i-1}^{\alpha} \rightarrow {}^{15}N_i(t_2) \rightarrow {}^1H_i^N(t_3)$$

and

$$^1H_i^N \rightarrow {}^{15}N_i \rightarrow {}^{13}C_{i,i-1}^{\alpha} \rightarrow {}^{13}C_{i,i-1}^{\alpha\beta\gamma\delta\varepsilon}(t_1) \rightarrow {}^{13}C_{i,i-1}^{\alpha}(t_3) \rightarrow {}^{15}N_i(t_2) \rightarrow {}^1H_i^N(t_4),$$

respectively. Conceptually the sequence is related to HNCACB (*42*) or HNCACBCG (*43, 44*) sequences where a magnetization transfer between backbone amide and side-chain $^{13}C^{\beta}$

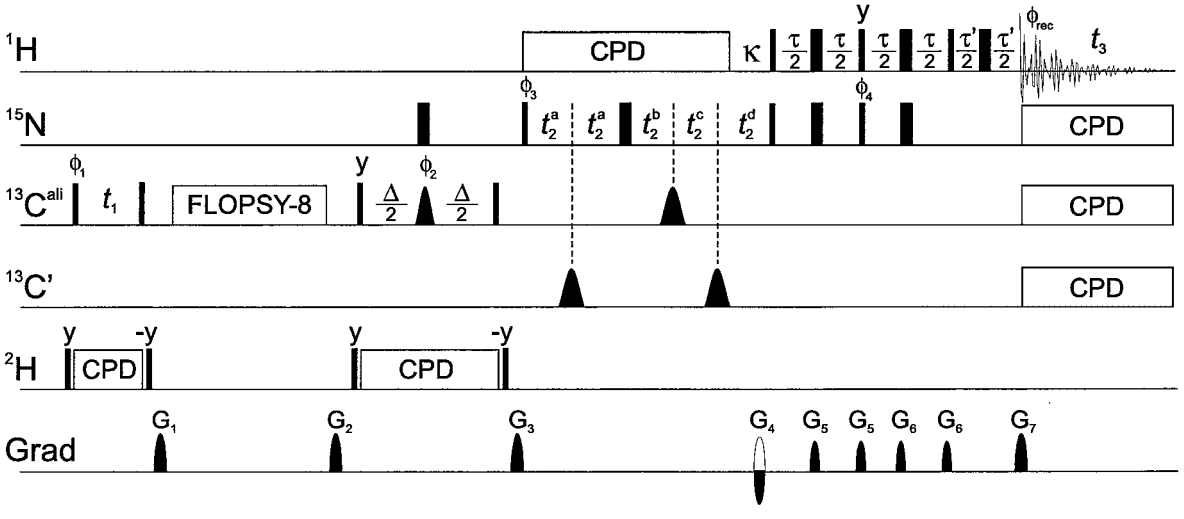

FIG. 1. Pulse sequence of the CC(CA)NH-TOCSY experiment. Narrow and wide filled rectangles denote 90° and 180° pulses, respectively. Carrier offsets are 4.75 (^{1}H), 118.0 (^{15}N), 41.6 (^{13}C), and 3.0 ppm (^{2}H). Off-resonance carbon pulses use phase-modulation of the carrier (*27*). Hard ^{1}H and ^{15}N pulses are applied with RF fields strengths of 28 and 7.8 kHz, respectively, while power levels are reduced to 5 kHz for ^{1}H DIPSI-2 (*28*) and 0.8 kHz for ^{15}N GARP-1 (*29*) composite pulse decoupling. Aliphatic carbon 90° pulses are rectangular (17.5 kHz RF field) and 180° pulses are G^3 Gaussian cascades (*30*) with durations of 220 and 350 μs, respectively, for the first and second one, where the latter pulse is centered in the $^{13}C^{\alpha}$ region (56 ppm). Isotropic mixing of ^{13}C magnetization is achieved with the FLOPSY-8 sequence (*31*) at an RF field strength of 7.8 kHz. Carbonyl 180° pulses are applied at 176 ppm and have the shape of the center lobe of a $\sin(x)/x$ function with a duration of 120 μs. ^{13}C decoupling during acquisition is accomplished by a sequence of adiabatic frequency-swept WURST (*32*) pulses (50 kHz sweep, 3-ms duration) centered at 108 ppm and employing a five-step supercycle (*33*). Deuterium composite pulse decoupling employs the WALTZ-16 sequence (*34*) applied along the x-axis at an RF field of 0.8 kHz. Delays Δ, κ, τ, and τ' are adjusted to 27, 5.4, 4.5, and 0.8 ms, respectively. Evolution of nitrogen chemical shifts is implemented in time in a semiconstant manner, where $t_2^a = (T_N - \chi t_2)/4$, $t_2^b = (1-\chi)t_2/2$, $t_2^c = (T_N + \chi t_2)/4$, $t_2^d = (T_N + (2-\chi)t_2)/4$, and $T_N = 24$ ms. The factor χ can vary between 0 and 1, depending on the desired ^{15}N acquisition time. Unless specified, pulses are applied along the x-axis. Phases are cycled according to $\phi_1 = 4(x), 4(-x); \phi_2 = x, y, -x, -y; \phi_3 = 2(x), 2(-x); \phi_4 = y; \phi_{\text{receiver}} = x, 2(-x), x, -x, 2(x), -x$. Sign discrimination in the F_1 dimension is accomplished by States–TPPI (*35*) of phase ϕ_1. Gradients are sine-bell shaped and have the following durations, peak amplitudes, and directions: G_1, 0.5 ms, 5 G/cm, y; G_2, 0.5 ms, 5 G/cm, z; G_3, 0.5 ms, 5 G/cm, x; G_4, 1.6 ms, −19.73 G/cm, xyz; G_5, 0.3 ms, 4 G/cm, xy; G_6, 0.3 ms, 5.5 G/cm, xy; G_7, 0.2 ms, 16 G/cm, xyz. Echo- and antiecho coherence transfer pathways are selected alternately by inversion of the polarity of G_4 along with the pulse phase ϕ_4. For each successive t_2 value, ϕ_3 and the receiver phase are incremented by 180°.

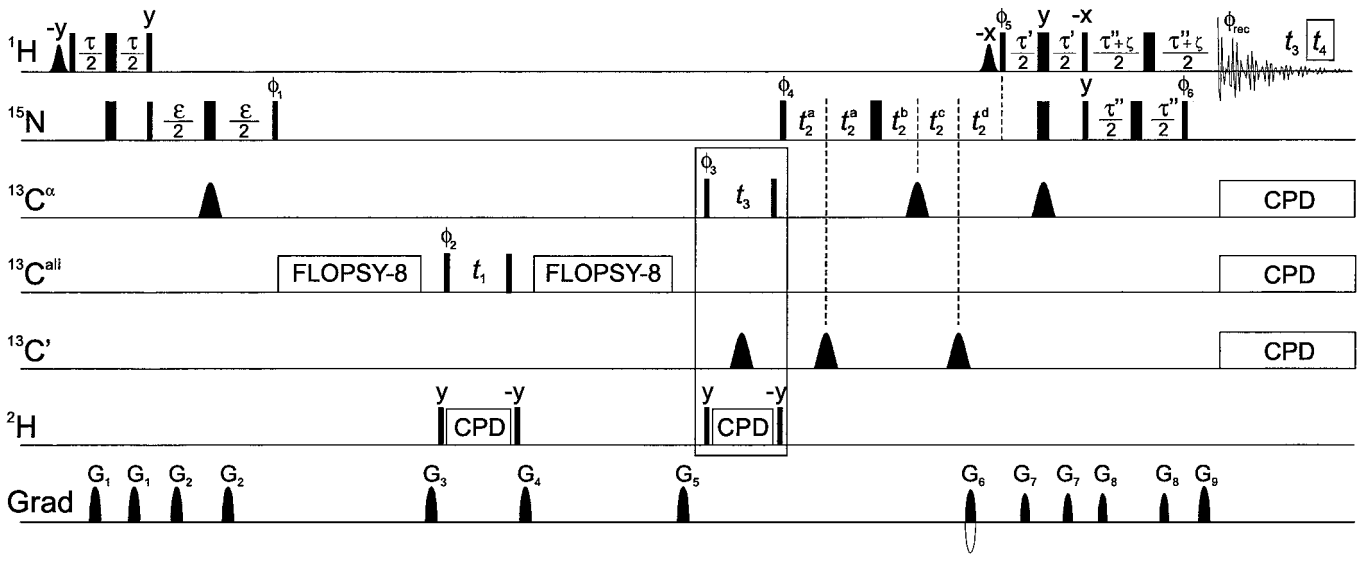

FIG. 2. Combined schemes for recording 3D (HNCAC)C(CCA)NH-TOCSY and 4D (HNCAC)C(C)CANH-TOCSY spectra. Narrow and wide bars denote RF pulses with flip angles of 90° and 180°, respectively, applied along the x-axis unless indicated otherwise. Pulses drawn in the box are only applied in the 4D version, where the acquisition time corresponds to t_4. In the 3D version, the pulse of phase ϕ_4 immediately follows gradient G_5, and t_3 is the ^{1}H acquisition rather than a $^{13}C^\alpha$ evolution period. The ^{1}H, ^{15}N, ^{13}C, and ^{2}H carrier positions are 4.75 (water), 118.0, 41.6, and 3.0 ppm, respectively, except for the t_3 period and the flanking 90° pulses in the 4D sequence, where the ^{13}C carrier is moved to 57.5 ppm. Rectangular proton pulses are applied with a 28-kHz RF field, while selective water flip-back pulses have a Gaussian shape, truncated at 10%, and a duration of 3 ms. Field strengths are 7.8 and 0.8 kHz for pulses on ^{15}N and ^{2}H (WALTZ-16 decoupling), respectively. Rectangular ^{13}C 90° pulses applied on aliphatic and α-carbons employ RF fields of 17.5 kHz and $\Delta/\sqrt{15}$, respectively, where Δ is the difference in Hz between the centers of the $^{13}C^\alpha$ and $^{13}C'$ regions (*39*). For the FLOPSY-8 mixing sequences, the field strength is adjusted to 7.8 kHz. Shaped 180° $^{13}C^\alpha$ pulses, applied at 56 ppm, are 350-μs G^3 Gaussian cascades, while $^{13}C'$ inversion pulses, applied at 176 ppm, are sinc-shaped and have a duration of 120 μs. Carbon decoupling during acquisition is implemented as a sequence of 3-ms WURST-20 pulses, applied at 108 ppm. Fixed delays are $\tau = 4.6$ ms, $\varepsilon = 24$ ms, $\tau' = 4.3$ ms, $\tau'' = 5.4$ ms, and $\zeta = 0.4$ ms. The initial duration of each of the periods t_2^a, t_2^c, and t_2^d is $T_N/4$ ($T_N = \varepsilon - \tau'$), while t_2^b is zero. Nitrogen chemical shifts evolve in time in a semiconstant manner according to $t_2^a = (T_N - \chi t_2)/4$, $t_2^b = (1-\chi)t_2/2$, $t_2^c = (T_N + \chi t_2)/4$, $t_2^d = (T_N + (2-\chi)t_2)/4$, where the factor χ is given by $T_N/t_{2\,max}$ ($t_{2\,max}$ being the desired ^{15}N acquisition time), if $t_{2\,max} > T_N$, otherwise $\chi = 1$. Phases are cycled as follows: $\phi_1 = 2(y), 2(-y); \phi_2 = x, -x; \phi_4 = 4(y), 4(-y); \phi_5 = y; \phi_6 = x; \phi_{receiver} = x, 2(-x), x, -x, 2(x), -x$ in the 3D version and $\phi_1 = y; \phi_2 = x, -x; \phi_3 = 2(x), 2(-x); \phi_4 = y; \phi_5 = y; \phi_6 = x; \phi_{receiver} = x, 2(-x), x$ in the 4D version. The phases of the first selective $(-y)$ and the second rectangular 90° (y) ^{1}H pulses are valid for applications on Bruker spectrometers, whereas they have to be inverted on Varian spectrometers (*40*) in order to constructively add components originating from ^{1}H and ^{15}N steady-state magnetization (*6, 41*). The sine-bell shaped gradients have the following durations, peak amplitudes, and directions: G_1, 0.5 ms, 5 G/cm, x; G_2, 0.5 ms, 5 G/cm, z; G_3, 0.5 ms, 5 G/cm, y; G_4, 0.5 ms, 6 G/cm, z; G_5, 0.5 ms, 7.5 G/cm, x; G_6, 1.6 ms, 19.73 G/cm, xyz; G_7, 0.3 ms, 4 G/cm, xy; G_8, 0.3 ms, 5.5 G/cm, xy; G_9, 0.2 ms, 16 G/cm, xyz. For each t_2 increment, N- and P-type transients are collected alternately by inverting the polarity of G_6 along with pulse phases ϕ_5 and ϕ_6. The two transients are stored separately and then added and subtracted to form the real and imaginary parts of a complex FID with a 90° zero-order phase shift being added to one of the components. Axial peaks in the ^{15}N dimension are shifted to the edge of the spectrum by incrementing ϕ_4 and the receiver phase by 180° for each value of t_2. Quadrature detection in t_1 (t_1 and t_3 in the 4D version) is accomplished by altering ϕ_2 (ϕ_2 and ϕ_3) in the States–TPPI manner.

or $^{13}C^\gamma$ resonances is accomplished in an out-and-back manner, making them readily applicable to perdeuterated proteins. However, complete aliphatic side-chain assignments can only be achieved with the (HNCAC)C(C)CANH-TOCSY method. Carbon–carbon isotropic mixing employed here for the transfer from $^{13}C^\alpha$ into the side-chain and—after chemical shift labeling—back to $^{13}C^\alpha$ is preferable over a multiple step carbon–carbon COSY scheme because it is faster and less prone to transverse relaxation. The (HNCAC)C(C)CANH-TOCSY takes advantage of the sensitivity enhanced [^{15}N, ^{1}H]-TROSY detection scheme (*40, 45–50*) to attenuate nitrogen and proton R_2 relaxation. In the present implementation gradient echo–antiecho coherence selection is employed and the number of ^{1}H 180° pulses is minimized in a manner described previously (*51*). The final $^{13}C^\alpha$ inversion pulse serves to concatenate the τ' period of the TROSY scheme with the $^{13}C^\alpha \rightarrow {}^{15}$N back transfer in order to reduce the length of the sequence (*52, 53*). Water-selective pulses are applied in the usual manner to ensure minimal saturation of fast-exchanging amide protons (*54–56*).

Compared to the CC(CA)NH-TOCSY scheme, the (HNCAC)C(C)CANH-TOCSY is favored in terms of sensitivity, as it utilizes steady state magnetization of both ^{1}H and ^{15}N rather than the considerably smaller polarization of carbons. With respect to potential losses due to relaxation, the overall duration of the (HNCAC)C(C)CANH-TOCSY sequence is obviously longer due to the second CC isotropic mixing period. Note that during this period ^{13}C magnetization decays with an average of R_1 and R_2 relaxation rates rather than pure transverse relaxation as in the case of free precession periods in CC COSY steps. The additional $^{15}N \rightarrow {}^{13}C^\alpha$ transfer delay ε is more than counterbalanced by the omission of the

Δ interval for $^{13}C^{\alpha} \rightarrow {}^{15}N$ transfer in the CC(CA)NH-TOCSY since transverse relaxation of the ^{15}N TROSY component is commonly slower than that of $^{13}C^{\alpha}$, even for perdeuterated proteins. It should be mentioned that the CC(CA)NH-TOCSY can be modified to include a [^{15}N, ^{1}H]-TROSY element. However, in the present application at a moderate magnetic field strength (600-MHz proton frequency), this resulted in a slightly decreased sensitivity compared to the non-TROSY pulse scheme of Fig. 1, which can be attributed to the "out-and-stay" type magnetization transfer pathway which does not allow inclusion of the native ^{15}N magnetization and involves only half the duration of transverse ^{15}N magnetization as the (HNCAC)C(C)CANH-TOCSY.

The utility of the novel methods has been tested with a completely deuterated, $^{13}C/^{15}N$-labeled sample of diisopropylfluorophosphatase (DFPase) from *Loligo vulgaris*, a 35-kDa protein consisting of a single polypeptide chain of 314 amino acid residues. Figure 3 compares spectra obtained under identical conditions using the 3D CC(CA)NH-TOCSY and (HNCAC)C(CCA)NH-TOCSY pulse sequences at 600-MHz proton Larmor frequency. As can be seen for almost all residue types, a number of backbone amide to side-chain carbon correlations are already obtained in the CC(CA)NH-TOCSY experiment. However, some of the expected, in particular the usually weaker interresidual cross peaks are missing due to sensitivity reasons. More complete correlation maps are observed in the corresponding strips from the 3D (HNCAC)C(CCA)NH-TOCSY spectrum. The examples chosen include residues from well-ordered and more dynamic regions of the protein structure, although it should be mentioned that DFPase has a markedly high content of β-sheet secondary structure, lacking any unstructured regions, and only moderate variations in linewidths are observed in the spectra. As is the case for other pulse sequences, the experiments proposed here do not perform equally well for residues with narrow and broad lines. In this respect no systematic differences were found between the CC(CA)NH-TOCSY and the (HNCAC)C(CCA)NH-TOCSY methods. Typically, the signal-to-noise is 1.5 to 2 times higher in the latter experiment, in accordance with expectations based on the different magnetization transfer pathways.

A drawback of the (HNCAC)C(C)CANH-TOCSY sequence is that the effect of a nonuniform transfer efficiency, inherent to commonly used CC-TOCSY mixing schemes, is exacerbated because such periods are employed twice. As a consequence, relatively large intensity differences within the same side-chain are encountered and, depending on the mixing time chosen, some positions tend to give very weak signals. In rare cases, cross peaks (e.g., Lys58 C^{ε} and Gln98 C^{β} in Fig. 3) were even absent in the (HNCAC)C(CCA)NH-TOCSY whereas they could be observed in the CC(CA)NH-TOCSY spectrum.

In contrast to (H)CC(CO)NH-TOCSY based sequences the experiments proposed here are able to provide side-chain resonance assignments for residues sequentially preceding prolines, such as Ile3 in Fig. 3. Furthermore, it is possible to link arginine ε-nitrogen and -proton to intraresidual carbon resonances, allowing for their sequence-specific assignment by comparison with cross-peak patterns obtained for arginine backbone sites. As pointed out previously (*57, 58*) such assignments are crucial for the determination of global folds of perdeuterated proteins owing to their low proton densities and concomitant limited number of available NOEs.

Similar to other NH-detected three-dimensional experiments, problems arise whenever chemical shifts of two or more amino acids are degenerate in both the $^{1}H^{N}$ and the ^{15}N dimensions. Likewise, distinctions between intra- and interresidual correlations in 3D (HNCAC)C(CCA)NH-TOCSY or CC(CA)NH-TOCSY spectra cannot always be made based on cross-peak intensities even though the intraresidual transfer is favored owing to the usually larger $^{1}J_{NC_{\alpha}}$ coupling constant. This is a consequence of the nonuniform transfer efficiency brought about by ^{13}C isotropic mixing, as mentioned above. As a remedy, the dispersion of $^{13}C^{\alpha}$ chemical shifts may be exploited to separate intra- and interresidual correlations or to resolve overlapping amides. To this end the 3D (HNCAC)C(CCA)NH-TOCSY sequence has been extended to a 4D (HNCAC)C(C)CANH-TOCSY pulse scheme simply by inserting a $^{13}C^{\alpha}$ (t_3) evolution time before the $^{13}C^{\alpha} \rightarrow {}^{15}N$ back transfer, as indicated in Fig. 2.

The utility of a 4D (HNCAC)C(C)CANH-TOCSY spectrum is demonstrated in Fig. 4, showing typical cases of ambiguous assignments in the 3D version of the experiment. For instance, for residue pair Leu9/Pro8 it was not obvious from cross-peak intensities in the 3D (HNCAC)C(CCA)NH-TOCSY which correlations are intraresidual and which are interresidual. A distinction can, however, be readily made in the 4D (HNCAC)C(C)CANH-TOCSY, where the two types are separated along the $^{13}C^{\alpha}$ (ω_3) dimension. The 4D spectrum furthermore revealed the near-degeneracy of Leu9 $^{13}C^{\gamma}$ and Pro8 $^{13}C^{\beta}$ chemical shifts, giving rise to overlap in the 3D (HNCAC)C(CCA)NH-TOCSY. Similarly, partial overlap between the Val66 $^{13}C^{\beta}$/Glu65 $^{13}C^{\gamma}$ and Met164 $^{13}C^{\gamma}$/Gln163 $^{13}C^{\gamma}$ cross peaks present in the 3D (HNCAC)C(CCA)NH-TOCSY is resolved in the 4D variant, at the same time allowing their unambiguous assignment to residues i or $i-1$. In the case of Lys214/Asn213, additional complications arise from the fact that the amide ^{1}H and ^{15}N chemical shifts of Lys214 almost coincide with those of Leu309, such that the corresponding cross section along the ^{13}C dimension in the 3D spectrum potentially contains correlations from four different side-chains. These are spread along the ω_3-axis in the 4D (HNCAC)C(C)CANH-TOCSY according to the respective $^{13}C^{\alpha}$ resonance frequencies, and the identification of cross peaks belonging to Lys214 and Asn213 becomes straightforward. On the other hand, a disadvantage of the 4D method is its inherently lower sensitivity, which, ignoring relaxation effects, is reduced by a factor of $2^{1/2}$ compared to the 3D version. Some weak cross peaks in the 3D (HNCAC)C(CCA)NH-TOCSY spectrum, e.g., Met164 and Gln163 $^{13}C^{\beta}$ or Leu309 $^{13}C^{\delta}$, were therefore not detected in the 4D spectrum.

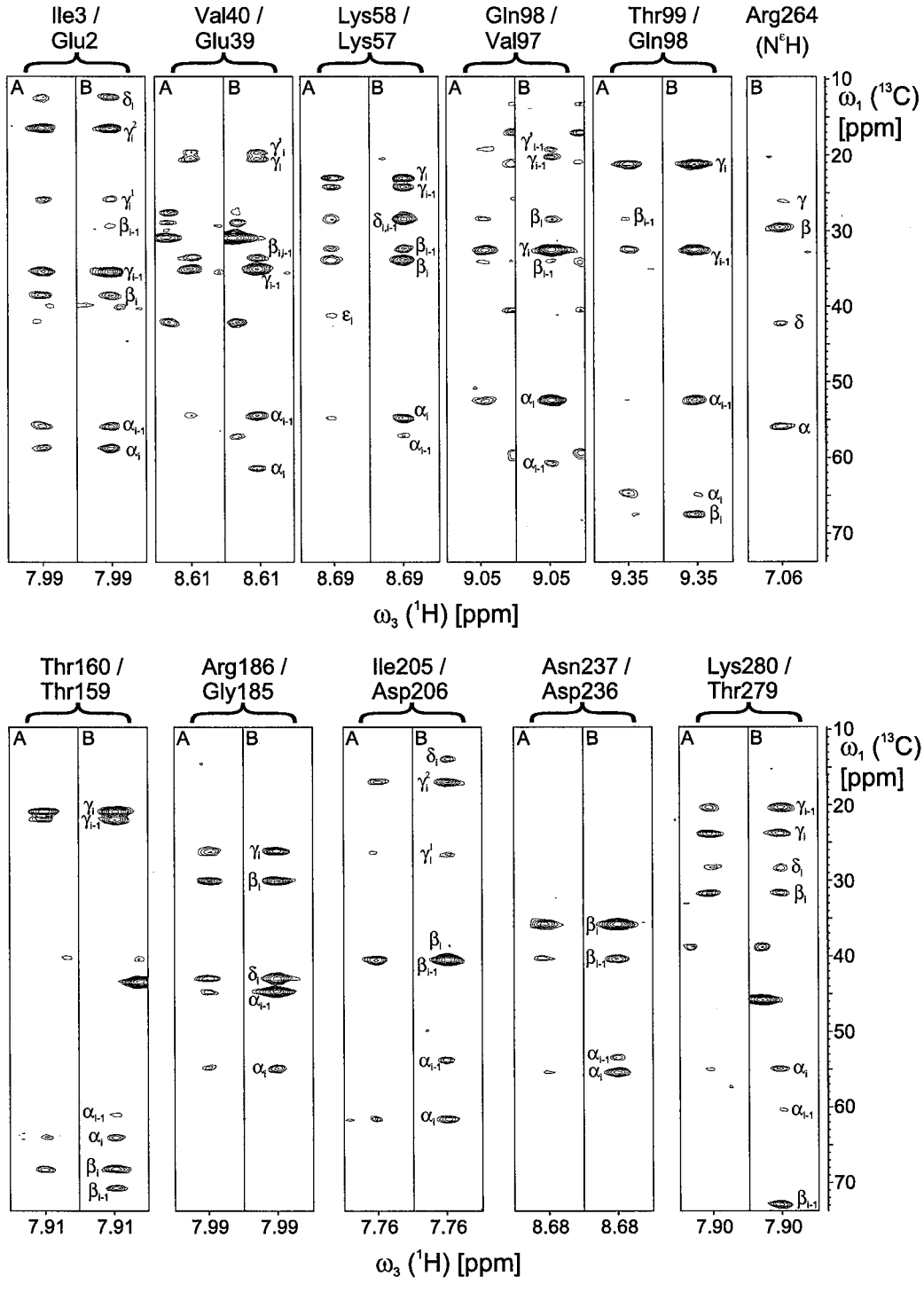

FIG. 3. Sections of $^{13}C/^1H^N(\omega_1/\omega_3)$ slices from 3D CC(CA)NH-TOCSY (A) and 3D (HNCAC)C(CCA)NH-TOCSY (B) spectra of $^2H/^{13}C/^{15}N$-labeled DFPase, taken at the backbone ^{15}N (ω_2) chemical shifts of residues i, the pairs $i, i-1$ given at the top of each panel. As an exception the strip from the (HNCAC)C(CCA)NH-TOCSY, containing correlations within the Arg264 side-chain, is extracted at the position of the ε-nitrogen resonance. The corresponding cross peaks in the CC(CA)NH-TOCSY (not shown) are severely broadened along the proton dimension due to incomplete nitrogen decoupling as a result of their large offset from the ^{15}N carrier. Each strip has a width of 0.15 ppm along ω_3 and is centered around the chemical shift indicated at the bottom. To assess the relative signal-to-noise ratios, contour levels are drawn on an exponential scale using a factor of $2^{1/2}$, the lowest being just above the noise level in both spectra. Carbon-13 resonance assignments are indicated by the respective positions in the side-chains of residues i and $i-1$, drawn in the (HNCAC)C(CCA)NH-TOCSY slices unless cross peaks appeared in the CC(CA)NH-TOCSY only. Stereospecific assignments of valine methyl groups (denoted γ and γ') are not available.

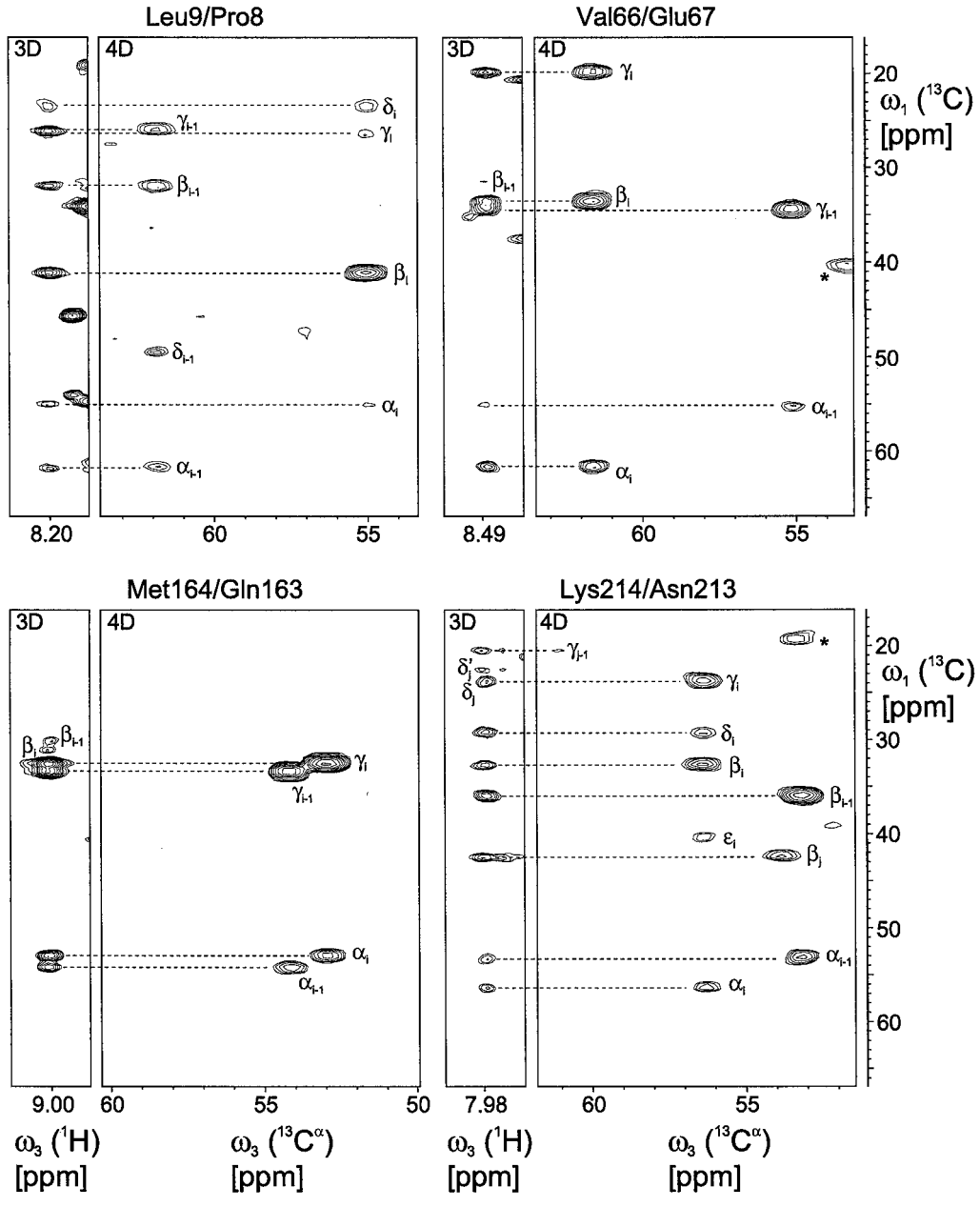

FIG. 4. Four examples showing the resolution of overlap in (HNCAC)C(C)CANH-TOCSY spectra of $^{2}H/^{13}C/^{15}N$-labeled DFPase. For each residue pair $i/i-1$ a $^{13}C/^{1}H^{N}$ (ω_1/ω_3) strip (0.15 ppm width) from the 3D (HNCAC)C(CCA)NH-TOCSY, taken at the ^{15}N (ω_2) chemical shift of residue i, is plotted at the left side and the corresponding $^{13}C/^{13}C^{\alpha}$ (ω_1/ω_3) plane at the $^{15}N/^{1}H^{N}$ (ω_2/ω_4) chemical shifts of the same residue in the 4D (HNCAC)C(C)CANH-TOCSY is shown at the right. Dashed lines connect equivalent cross peaks present in both spectra. Cross peaks belonging to other residues which have their maximal intensity in neighboring slices are marked by asterisks. In the lower right panel (Lys214/Asn213), cross peaks labeled β_j, γ_{j-1}, δ_j, and δ'_j have been assigned to Leu309/Thr308.

CONCLUSIONS

Pulse sequences have been introduced allowing side-chain ^{13}C resonance assignments to be obtained in larger, perdeuterated proteins. Employing aliphatic carbons as the initial source of magnetization, the CC(CA)NH-TOCSY scheme represents the intraresidual analogue of the CC(CO)NH-TOCSY (*24*). In cases where fast transverse ^{13}CO relaxation degrades the efficiency of the carbonyl-relayed $^{13}C^{\alpha} \rightarrow {}^{15}N$ transfer in the latter experiment, the CC(CA)NH-TOCSY might be an alternative to link side-chain ^{13}C to backbone amide chemical shifts. A considerably higher sensitivity is, however, achieved with the out-and-back type (HNCAC)C(CCA)NH-TOCSY pulse scheme which exploits the sum of ^{1}H and ^{15}N rather than ^{13}C polarization

and takes advantage of TROSY enhancement. Owing to the branched magnetization transfer pathway the new methods complement the HNCACB experiment (*42*), at the same time providing sequential connectivities and side-chain chemical shift information.

EXPERIMENTAL

Triply labeled DFPase was expressed in *E.coli* grown on a diluted $^{2}H/^{13}C/^{15}N$-enriched (>96%), algal lysate based medium (Cambridge Isotope Laboratories, Inc., Andover, MA), supplemented with 1 g/l $^{2}H_7/^{13}C_6$ glucose (>97%) (Martek Biosciences Corp., Columbia, MD) and 1 g/l $^{15}NH_4Cl$ (>98%) (Martek). The sample concentration was 0.9 mM in 10-mM Bis-Tris–propane (1,3-bis[tris-(hydroxymethyl-)methylamino]-propane) buffer (95% H_2O/5% D_2O) at pH 6.3. All data sets were recorded at a temperature of 28°C on a four-channel 600-MHz Bruker Avance spectrometer, equipped with a 5-mm three-axis gradient $^{1}H\{^{13}C, ^{15}N\}$-triple resonance probe.

Three-dimensional CC(CA)NH-TOCSY and (HNCAC)C(CCA)NH-TOCSY spectra were acquired with spectral widths of 64.3 ppm along F_1 (^{13}C), 20.0 ppm along F_2 (^{15}N), and 10.3 ppm along F_3 (^{1}H). Time domain data consisted of $70 \times 48 \times 512$ (t_1, t_2, t_3) complex points, corresponding to acquisition times of 7.3, 39.5, and 82.8 ms, respectively, the values of the semiconstant time factors χ being 0.62 in the CC(CA)NH-TOCSY and 0.51 in the (HNCAC)C(CCA)NH-TOCSY. Accumulation of eight scans per FID resulted in recording times of 69 h for each data set. In the four-dimensional (HNCAC)C(C)CANH-TOCSY experiment spectral widths comprised 59.7 (F_1, ^{13}C), 10.0 (F_2, ^{15}N), 15.4 (F_3, $^{13}C^{\alpha}$), and 10.3 ppm (F_4, ^{1}H). Acquisition times (number of complex data points) were 4.7 (42), 16.4 (10), 6.9 (16), and 82.8 ms (512) in t_1, t_2, t_3, and t_4, respectively, such that it could be recorded as a constant-time (i.e., $\chi = 1$) version with respect to the ^{15}N domain. The spectrum was acquired within 132 h, using four scans per FID. In all experiments, the length of the TOCSY mixing period was adjusted to 18.1 ms, corresponding to six cycles of FLOPSY-8.

Processing and spectra analysis was carried out using the NMRPipe/NMRDraw (*59*) software. Linear prediction was employed to extend acquisition data in all indirect dimensions by approximately 1/3 of their original length. Prior to Fourier transformation, time domain data were apodized with squared-cosine functions in all dimensions. Zero-filling was applied to obtain final 3D and 4D data set sizes of $256 \times 128 \times 512$ and $128 \times 32 \times 64 \times 512$ points, respectively, retaining only the low-field half in the ^{1}H dimension.

ACKNOWLEDGMENTS

The authors thank Dr. Judith Hartleib for the preparation of the labeled DFPase sample. All spectra were recorded at the Large Scale Facility for Biomolecular NMR at the University of Frankfurt. This work was supported by a grant from the Fraunhofer-Gesellschaft (E/B31E/M0157/M5137).

REFERENCES

1. L. E. Kay and K. H. Gardner, Solution NMR spectroscopy beyond 25 kDa, *Curr. Opin. Struct. Biol.* **7,** 722–731 (1997).
2. K. H. Gardner and L. E. Kay, The use of ^{2}H, ^{13}C, ^{15}N multidimensional NMR to study the structure and dynamics of proteins, *Annu. Rev. Biophys. Biomol. Struct.* **27,** 357–406 (1998).
3. B. T. Farmer II and R. A. Venters, NMR of perdeuterated large proteins, *in* "Biological Magnetic Resonance, Vol. 16: Modern Techniques in Protein NMR" (N. R. Krishna and L. J. Berliner, Eds.), pp. 75–120, Kluwer Academic/Plenum, New York (1998).
4. S. Grzesiek, J. Anglister, H. Ren, and A. Bax, ^{13}C line narrowing by ^{2}H decoupling in $^{2}H/^{13}C/^{15}N$-enriched proteins: Application to triple resonance 4D *J* connectivity of sequential amides, *J. Am. Chem. Soc.* **115,** 4369–4370 (1993).
5. T. Yamazaki, W. Lee, C. H. Arrowsmith, D. R. Muhandiram, and L. E. Kay, A suite of triple resonance NMR experiments for the backbone assignment of ^{15}N, ^{13}C, ^{2}H labeled proteins with high sensitivity, *J. Am. Chem. Soc.* **116,** 11655–11666 (1994).
6. K. Pervushin, R. Riek, G. Wider, and K. Wüthrich, Attenuated T_2 relaxation by mutual cancellation of dipole-dipole coupling and chemical shift anisotropy indicates an avenue to NMR structures of very large biological macromolecules in solution, *Proc. Natl. Acad. Sci. USA* **94,** 12366–12371 (1997).
7. M. Salzmann, K. Pervushin, G. Wider, H. Senn, and K. Wüthrich, TROSY in triple-resonance experiments: New perspectives for sequential NMR assignment of large proteins, *Proc. Natl. Acad. Sci. USA* **95,** 13585–13590 (1998).
8. M. Salzmann, G. Wider, K. Pervushin, H. Senn, and K. Wüthrich, TROSY-type triple-resonance experiments for sequential NMR assignments in large proteins, *J. Am. Chem. Soc.* **121,** 844–848 (1999).
9. D. Yang and L. E. Kay, TROSY triple-resonance four-dimensional NMR spectroscopy of a 46 ns tumbling protein, *J. Am. Chem. Soc.* **121,** 2571–2575 (1999).
10. R. Konrat, D. Yang, and L. E. Kay, A 4D TROSY-based pulse scheme for correlating $^{1}HN_i$, $^{15}N_i$, $^{13}C_i^{\alpha}$, $^{13}C'_{i-1}$ chemical shifts in high molecular weight, ^{15}N, ^{13}C, ^{2}H labeled proteins, *J. Biomol. NMR* **15,** 309–313 (1999).
11. F. A. A. Mulder, A. Ayed, D. Yang, C. H. Arrowsmith, and L. E. Kay, Assignment of $^{1}H^{N}$, ^{15}N, $^{13}C^{\alpha}$, ^{13}CO and $^{13}C^{\beta}$ resonances in a 67 kDa p53 dimer using 4D-TROSY NMR spectroscopy, *J. Biomol. NMR* **18,** 173–176 (2000).
12. M. Salzmann, K. Pervushin, G. Wider, H. Senn, and K. Wüthrich, NMR assignment and secondary structure determination of an octameric 110 kDa protein using TROSY in triple resonance experiments, *J. Am. Chem. Soc.* **122,** 7543–7548 (2000).
13. G. T. Montelione, B. A. Lyons, S. D. Emerson, and M. Tashiro, An efficient triple resonance experiment using carbon-13 isotropic mixing for determining sequence-specific resonance assignments of isotopically-enriched proteins, *J. Am. Chem. Soc.* **114,** 10974–10975 (1992).
14. T. M. Logan, E. T. Olejniczak, R. X. Xu, and S. W. Fesik, Side chain and backbone assignments in isotopically labeled proteins from two heteronuclear triple resonance experiments, *FEBS Lett.* **314,** 413–418 (1992).
15. S. Grzesiek, J. Anglister, and A. Bax, Correlation of backbone amide and aliphatic side-chain resonances in $^{13}C/^{15}N$-enriched proteins by isotropic mixing of ^{13}C magnetization, *J. Magn. Reson. Ser. B* **101,** 114–119 (1993).

16. R. T. Clowes, W. Boucher, C. H. Hardman, P. J. Domaille, and E. D. Laue, A 4D HCC(CO)NNH experiment for the correlation of aliphatic side-chain and backbone resonances in $^{13}C/^{15}N$-labelled proteins, *J. Biomol. NMR* **3,** 349–354 (1993).
17. D. Nietlispach, R. T. Clowes, R. W. Broadhurst, Y. Ito, J. Keeler, M. Kelly, J. Ashurst, H. Oschkinat, P. J. Domaille, and E. D. Laue, An approach to the structure determination of larger proteins using triple resonance NMR experiments in conjunction with random fractional deuteration, *J. Am. Chem. Soc.* **118,** 407–415 (1996).
18. Y. Lin and G. Wagner, Efficient side-chain and backbone assignment in large proteins: Application to tGCN5, *J. Biomol. NMR* **15,** 227–239 (1999).
19. K. H. Gardner, R. Konrat, M. R. Rosen, and L. E. Kay, An (H)C(CO)NH-TOCSY pulse scheme for sequential assignment of protonated methyl groups in otherwise deuterated ^{15}N, ^{13}C-labeled proteins, *J. Biomol. NMR* **8,** 351–356 (1996).
20. K. H. Gardner, X. Zhang, K. Gehring, and L. E. Kay, Solution NMR studies of a 42 kDa *Escherichia coli* maltose binding protein/β-cyclodextrin complex: Chemical shift assignments and analysis, *J. Am. Chem. Soc.* **120,** 11738–11748 (1998).
21. M. K. Rosen, K. H. Gardner, R. C. Willis, W. E. Parris, T. Pawson, and L. E. Kay, Selective methyl group protonation of perdeuterated proteins, *J. Mol. Biol.* **263,** 627–636 (1996).
22. K. H. Gardner and L. E. Kay, Production and incorporation of ^{15}N, ^{13}C, ^{2}H (^{1}H-δ1 methyl) isoleucine into proteins for multidimensional NMR studies, *J. Am. Chem. Soc.* **119,** 7599–7600 (1997).
23. N. K. Goto, K. H. Gardner, G. A. Mueller, R. C. Willis, and L. E. Kay, A robust and cost-effective method for the production of Val, Leu, Ile (δ1) methyl-protonated ^{15}N-, ^{13}C-, ^{2}H-labeled proteins, *J. Biomol. NMR* **13,** 369–374 (1999).
24. B. T. Farmer II and R. A. Venters, Assignment of side-chain ^{13}C resonances in perdeuterated proteins, *J. Am. Chem. Soc.* **117,** 4187–4188 (1995).
25. G. A. Morris and R. Freeman, Enhancement of nuclear magnetic resonance signals by polarization transfer, *J. Am. Chem. Soc.* **101,** 760–762 (1979).
26. B. A. Lyons and G. T. Montelione, An HCCNH triple-resonance experiment using carbon-13 isotropic mixing for correlating backbone amide and side-chain aliphatic resonances in isotopically enriched proteins, *J. Magn. Reson. Ser. B* **101,** 206–209 (1993).
27. S. L. Patt, Single- and multiple-frequency-shifted laminar pulses, *J. Magn. Reson.* **96,** 94–102 (1992).
28. A. J. Shaka, C. J. Lee, and A. Pines, Iterative schemes for bilinear operators; application to spin decoupling, *J. Magn. Reson.* **77,** 274–293 (1988).
29. A. J. Shaka, P. B. Barker, and R. Freeman, Computer-optimized decoupling scheme for wideband applications and low-level operation, *J. Magn. Reson.* **64,** 547–552 (1985).
30. L. Emsley and G. Bodenhausen, Gaussian pulse cascades: New analytical functions for rectangular selective inversion and in-phase excitation in NMR, *Chem. Phys. Lett.* **165,** 469–476 (1990).
31. A. Mohebbi and A. J. Shaka, Improvements in carbon-13 broadband homonuclear cross-polarization for 2D and 3D NMR, *Chem. Phys. Lett.* **178,** 374–378 (1991).
32. Ē. Kupče and R. Freeman, Adiabatic pulses for wideband inversion and broadband decoupling, *J. Magn. Reson. Ser. A* **115,** 273–276 (1995).
33. R. Tycko, A. Pines, and R. Guckenheimer, Fixed point theory of iterative excitation schemes in NMR, *J. Chem. Phys.* **83,** 2775–2802 (1985).
34. A. J. Shaka, J. Keeler, T. Frenkiel, and R. Freeman, An improved sequence for broadband decoupling: WALTZ-16, *J. Magn. Reson.* **52,** 335–338 (1983).
35. D. Marion, M. Ikura, R. Tschudin, and A. Bax, Rapid recording of 2D NMR spectra without phase cycling. Application to the study of hydrogen exchange in proteins, *J. Magn. Reson.* **85,** 393–399 (1989).
36. S. Grzesiek and A. Bax, Amino acid type determination in the sequential assignment procedure of uniformly $^{13}C/^{15}N$-enriched proteins, *J. Biomol. NMR* **3,** 185–204 (1993).
37. A. G. Palmer III, J. Cavanagh, P. E. Wright, and M. Rance, Sensitivity improvement in proton-detected two-dimensional heteronuclear correlation spectroscopy, *J. Magn. Reson.* **93,** 151–170 (1991).
38. L. E. Kay, P. Keifer, and T. Saarinen, Pure absorption gradient enhanced heteronuclear single quantum correlation spectroscopy with improved sensitivity, *J. Am. Chem. Soc.* **114,** 10663–10665 (1992).
39. L. E. Kay, M. Ikura, R. Tschudin, and A. Bax, Three-dimensional triple-resonance NMR spectroscopy of isotopically enriched proteins, *J. Magn. Reson.* **89,** 496–514 (1990).
40. G. Zhu, X. M. Kong, X. Z. Yan, and K. H. Sze, Sensitivity enhancement in transverse relaxation optimized NMR spectroscopy, *Angew. Chem. Int. Ed. Engl.* **37,** 2859–2861 (1998).
41. K. Pervushin, R. Riek, G. Wider, and K. Wüthrich, Transverse relaxation-optimized spectroscopy (TROSY) for NMR studies of aromatic spin systems in ^{13}C-labeled proteins, *J. Am. Chem. Soc.* **120,** 6394–6400 (1998).
42. M. Wittekind and L. Mueller, HNCACB, a high-sensitivity 3D NMR experiment to correlate amide-proton and nitrogen resonances with the alpha- and beta-carbon resonances in proteins, *J. Magn. Reson. Ser. B* **101,** 201–205 (1993).
43. K. L. Constantine, L. Mueller, V. Goldfarb, M. Wittekind, W. J. Metzler, J. Yanchunas Jr, J. G. Robertson, M. F. Malley, M. S. Friedrichs, and B. T. Farmer II, Characterization of $NADP^+$ binding to perdeuterated MurB: Backbone atom NMR assignments and chemical-shift changes, *J. Mol. Biol.* **267,** 1223–1246 (1997).
44. S. A. McCallum, T. K. Hitchens, and G. S. Rule, Unambiguous correlations of backbone amide and aliphatic gamma resonances in deuterated proteins, *J. Magn. Reson.* **134,** 350–354 (1998).
45. M. Czisch and R. Boelens, Sensitivity enhancement in the TROSY experiment, *J. Magn. Reson.* **134,** 158–160 (1998).
46. P. Andersson, A. Annila, and G. Otting, An α/β-HSQC-α/β experiment for spin-state selective editing of IS cross-peaks, *J. Magn. Reson.* **133,** 364–367 (1998).
47. K. V. Pervushin, G. Wider, and K. Wüthrich, Single transition-to-single transition polarization transfer (ST2-PT) in [^{15}N, ^{1}H]-TROSY, *J. Biomol. NMR* **12,** 345–348 (1998).
48. M. Rance, J. P. Loria, and A. G. Palmer III, Sensitivity improvement of transverse relaxation-optimized spectroscopy, *J. Magn. Reson.* **136,** 92–101 (1999).
49. J. Weigelt, Single scan, sensitivity- and gradient-enhanced TROSY for multidimensional NMR experiments, *J. Am. Chem. Soc.* **120,** 10778–10779 (1998).
50. B. Brutscher, J. Boisbouvier, A. Pardi, D. Marion, and J.-P. Simorre, Improved sensitivity and resolution in ^{1}H-^{13}C NMR experiments of RNA, *J. Am. Chem. Soc.* **120,** 11845–11851 (1998).
51. A. J. Dingley and S. Grzesiek, Direct observation of hydrogen bonds in nucleic acid base pairs by internucleotide $^{2}J_{NN}$ couplings, *J. Am. Chem. Soc.* **120,** 8293–8297 (1998).
52. J. P. Loria, M. Rance, and A. G. Palmer III, Transverse-relaxation-optimized (TROSY) gradient-enhanced triple-resonance NMR spectroscopy. *J. Magn. Reson.* **141,** 180–184 (1999).
53. M. Salzmann, G. Wider, K. Pervushin, and K. Wüthrich, Improved sensitivity and coherence selection for [^{15}N, ^{1}H]-TROSY elements in triple resonance experiments, *J. Biomol. NMR* **15,** 181–184 (1999).

54. S. Grzesiek and A. Bax, The importance of not saturating H_2O in protein NMR. Application to sensitivity enhancement and NOE measurements, *J. Am. Chem. Soc.* **115,** 12593–12594 (1993).

55. J. Stonehouse, G. L. Shaw, J. Keeler, and E. D. Laue, Minimizing sensitivity losses in gradient-selected ^{15}N-^{1}H HSQC spectra of proteins, *J. Magn. Reson. Ser. A* **107,** 178–184 (1994).

56. H. Matsuo, Ē. Kupče, H. Li, and G. Wagner, Use of selective C^{α} pulses for improvement of HN(CA)CO-D and HN(COCA)NH-D experiments, *J. Magn. Reson. Ser. B* **111,** 194–198 (1996).

57. R. A. Venters, W. J. Metzler, L. D. Spicer, L. Mueller, and B. T. Farmer II, Use of $^{1}H^{N}$-$^{1}H^{N}$ NOEs to determine protein global folds in perdeuterated proteins, *J. Am. Chem. Soc.* **117,** 9592–9593 (1995).

58. B. T. Farmer II and R. A. Venters, Assignment of aliphatic side-chain $^{1}H^{N}/^{15}N$ resonances in perdeuterated proteins, *J. Biomol. NMR* **7,** 59–71 (1996).

59. F. Delaglio, S. Grzesiek, G. W. Vuister, G. Zhu, J. Pfeifer, and A. Bax, NMRPipe: A multidimensional spectral processing system based on UNIX pipes, *J. Biomol. NMR* **6,** 277–293 (1995).